The Astrophysical Journal, 777:26 (11pp), 2013 November 1 doi:10.1088/0004-637X/777/1/26

OPTICAL CONSTANTS OF NH_3 AND NH_3:N_2 AMORPHOUS ICES IN THE NEAR-INFRARED AND MID-INFRARED REGIONS

Alexandre Zanchet, Yamilet Rodríguez-Lazcano, Óscar Gálvez, Víctor J. Herrero, Rafael Escribano, and Belén Maté
Instituto de Estructura de la Materia, IEM-CSIC, Serrano 123, E-28006 Madrid, Spain; belen.mate@csic.es

Received 2013 April 15; accepted 2013 July 17; published 2013 October 10

ABSTRACT

Ammonia ice has been detected on different astrophysical media ranging from interstellar medium (ISM) particles to the surface of various icy bodies of our solar system, where nitrogen is also present. We have carried out a detailed study of amorphous NH_3 ice and NH_3:N_2 ice mixtures, based on infrared (IR) spectra in the mid-IR (MIR) and near-IR (NIR) regions, supported by theoretical quantum chemical calculations. Spectra of varying ice thicknesses were obtained and optical constants were calculated for amorphous NH_3 at 15 K and 30 K and for a NH_3:N_2 mixture at 15 K over a 500–7000 cm^{-1} spectral range. These spectra have improved accuracy over previous data, where available. Moreover, we also obtained absolute values for the band strengths of the more prominent IR features in both spectral regions. Our results indicate that the estimated NH_3 concentration in ISM ices should be scaled upward by ∼30%.

Key words: ISM: abundances – methods: laboratory: solid state – planets and satellites: composition – techniques: spectroscopic

Online-only material: color figures, supplemental data

1. INTRODUCTION

Nitrogen is the fourth most abundant element in the universe after H, O, and C (Snow & Witt 1996); ammonia (NH_3) and N_2 are its main carriers. In fact, ammonia was the first polyatomic molecule detected in space (Cheung et al. 1968), and in a recent detailed analysis of *Spitzer* c2d Legacy ice survey data, it was established that the average abundance of NH_3 in the ices of high- and low-mass protostars is roughly 5% with respect to water (Bottinelli et al. 2010; Öberg et al. 2011). Ammonia is also an abundant molecule in our solar system, where it has been detected in the atmospheres of the gas giants (Cochran & Cochran 1981; Hofstadter & Muhleman 1989; Lindal 1992; Wong et al. 2004). From observations of the NIR 2.2 μm band, solid phase ammonia has been identified on the surfaces of various icy bodies such as Enceladus (Emery et al. 2005), Miranda (Bauer et al. 2002), Charon (Brown & Calvin 2000), and the Kuiper Belt Object Quaoar (Jewitt & Luu 2004). The presence of ammonia ice on the surface of outer solar system bodies, where it is expected to be depleted by energetic particles or cosmic rays (Moore et al. 2007), suggests that these objects undergo internal activity that replenishes their surfaces with NH_3.

Even the highly volatile N_2 molecule can freeze at the low temperatures (less than 40 K) of the bodies in the outer regions of our solar system. When spectral observations are of sufficient quality, the presence of crystalline N_2 can be determined directly from its weak absorption band at 2.15 μm (Grundy et al. 1993). In other cases, its presence can be deduced indirectly from band shifts detected in the spectra of other molecular species. This "matrix shift" occurs when the molecules are dissolved in frozen N_2 and was first seen in the CH_4 spectrum of Triton (Cruikshank et al. 1993; Quirico et al. 1999) based on laboratory studies by Quirico & Schmitt (1997). CH_4 band shifts to lower frequencies have also been observed in the spectrum of Pluto (Douté et al. 1999), Quaoar (Licandro et al. 2006a), and Makemake (Licandro et al. 2006b). The coexistence of NH_3 and N_2 ices of solar system objects such as Enceladus or Charon is also thought to be very likely (Dalton 2010; Dalton et al. 2010).

Most of our knowledge of ice composition is derived from IR observations, and hence laboratory IR studies of the different ice carriers provide valuable information to interpret these observations. Solid ammonia can be obtained by deposition of ammonia vapor on a cold substrate. In this case, when the substrate temperature is below 50 K, an amorphous phase is formed, while a crystalline phase is obtained at higher temperatures (above 80 K). A metastable phase that grows between these temperatures has also been reported by Holt et al. (2004). The IR spectrum of ammonia ice has been investigated by a number of research groups. The first study was conducted by Reding & Hornig (1951), who recorded and assigned the MIR spectrum of crystalline ammonia at 83 K. In the 1970s and 1980s, other works reported IR spectra of the different phases of ammonia (Robertson et al. 1975; Pipes et al. 1978). Some discrepancies in the assignments of the IR spectra to different phases are still open to debate, as revealed in the works of Holt et al. (2004), Zheng & Kaiser (2007), and Dawes et al. (2007).

Other laboratory works, focused on the astrophysical relevance of these species, are those of D'Hendecourt & Allamandola (1986), who provided the integrated band strength of amorphous ammonia at 10 K; Kerkhof et al. (1999), who studied the band strength of NH_3 in H_2O:NH_3 mixtures; and, more recently, Moore et al. (2007), who reported the IR spectra of the stoichiometric hydrates of ammonia. Also, the MIR and NIR spectra from highly diluted to highly concentrated H_2O:NH_3 ice mixtures were investigated by Zheng et al. (2009). Band strengths of combination modes of NH_3 in the NIR in pure ices and in mixtures with H_2O or N_2 were estimated by Gerakines et al. (2005) and Richey & Gerakines (2012) from measurements spanning both the MIR and NIR regimes.

From the IR spectra, it is possible to extract the wavelength dependent complex refractive index of the ice, whose components are also known as optical constants. These magnitudes are very useful for the astrophysical community because they

allow the simulation of the diffuse reflection spectra measured from solar system object observations. A good, current compilation of the investigations conducted on NH_3 optical constants is presented in Howett et al. (2007). For the amorphous phase of NH_3, the most complete results, as far as we know, are those of Wood & Roux (1982). These authors reported optical constants of NH_3 at 20 K for the 2.7–20 μm spectral range.

In this paper, we studied the MIR and NIR spectra of pure ammonia at 15 K and the modifications of these spectra in mixtures of NH_3 with N_2. These data should be useful for assessing the presence of the IR inactive N_2 in objects where the two nitrogen carriers (NH_3 and N_2) coexist. In addition, we have conducted calculations of the IR spectra of NH_3 amorphous solids (pure and mixed with N_2) and compared them with experimental measurements. This comparison provides insights into the causes that may explain the different spectral shapes observed for the various samples. Moreover, based on our experiments, we have determined new and refined optical constants of amorphous ammonia ice, a species abundant in astrophysical ices, at 15 K and 30 K. In particular, we have studied the 7000–500 cm^{-1} (1.4–20 μm) spectral region, covering a broader spectral range than previously reported. We have also calculated the optical constants in the same spectral region for a 1:1.7 NH_3:N_2 mixture at 15 K and performed a thermal processing of the ice in order to understand the role of N_2 in the crystallization of NH_3.

2. EXPERIMENT

Ices of ammonia and mixtures with N_2 were generated by vapor deposition. The apparatus used has been previously described by Maté et al. (2003) and Herrero et al. (2010), and only a brief account will be given here. The experimental arrangement consists of a high vacuum chamber with background pressures in the 10^{-8} mbar range coupled with a closed-cycle helium cryostat. An IR transparent silicon window, mounted in close thermal contact with the cold finger of the cryostat, is used as a deposition substrate for the ice samples. The substrate temperature can be controlled between 15 K and 300 K by means of a heating foil and a Lakeshore temperature controller linked to two silicon diodes as temperature sensors. Pure NH_3 vapor (99.96%, Alphagaz) was introduced from the bottle into the chamber through a needle valve to backfill the chamber. For NH_3:N_2 (N_2, 99.999%, Alphagaz) mixtures, the gases were introduced directly from their bottles through independent lines. The stoichiometry of the deposit was controlled by means of a quadrupole mass spectrometer previously calibrated for each species. The deposition pressures were in the 10^{-5} mbar range and the growth rates of the deposits varied between 3 and 6 nm s^{-1}. Normal incidence transmission IR spectra of the deposits were collected with a Bruker Vertex70 FTIR spectrometer coupled with the vacuum chamber through a purged pathway and KBr windows. The entire MIR and NIR spectrum was measured by a single external mercury cadmium telluride detector reached through two different beamsplitters and sources that could be exchanged without disturbing the purged pathway. The spectra were obtained by co-adding 500 scans taken at 2 cm^{-1} spectral resolution. For thermal processing experiments, the ices where heated at 5 K $minute^{-1}$ up to 85 K.

The ice film thickness was measured by monitoring the interference pattern of a He–Ne laser beam incident on the growing ice film at $\theta_1 = 4.0 \pm 0.2^\circ$ from the surface normal, as described previously (Maté et al. 2003). The reflected light was detected by a photodiode and converted to a digital signal. Constructive and destructive interference could be observed between the reflections from the vacuum-ice and the ice-metal interfaces as the ice film grows. The ice film growth between two consecutive constructive (or destructive) interference fringes is given by

$$x = \frac{\lambda_0}{2n_0 \sin\theta_1}, \quad (1)$$

where λ_0 is the wavelength of the He–Ne laser (632.8 nm) and n_0 is the refractive index of the ice film at the laser wavelength. The refractive index n_0 can be estimated from the intensity ratio between the maxima and the minima of the interference pattern collected by the photodiode (Goodman 1978). For amorphous NH_3 ice, there are some n_0 values given in the literature that range from 1.37 (Wood & Roux 1982; 20 K) to 1.44 (Dawes et al. 2007; 25 K). From our experiments for pure NH_3 ices at 15 K and 30 K, we estimated n_0 values of 1.36 $\pm$ 0.01 and 1.38 $\pm$ 0.01, respectively, and 1.26 $\pm$ 0.01 for the NH_3:N_2 (1:1.7) mixture at 15 K. As far as we know, no previous n_0 values have been published for NH_3:N_2 mixtures. Accordingly, the thickness x grown per maximum is 233 nm, 230 nm, and 252 nm for pure NH_3 at 15 K, 30 K, and for the mixture, respectively. The absolute accuracy of the thickness determined in this way is $\sim$5% and it is limited mainly by errors in measuring the incidence angle of the laser and the refractive index n_0.

Pure amorphous NH_3 ices and NH_3:N_2 mixtures grown at 15 K present a higher optical quality, as inferred from the higher contrast of the He-Ne interference pattern. On the contrary, for pure NH_3 ices deposited at 30 K, only a few interference maxima could be measured, indicating that some film fracture or scattering phenomenon takes place above $\sim$1 μm, as was already reported in the literature (Wood & Roux 1982). We have also noticed that due to the fast growing rates used in our experiments, $\sim$5 nm s^{-1}, the temperature stability of the ices grown at 15 K is limited to ices up 2 μm thick. These facts limit the thickness of the samples used for the determination of optical constants. To take this into account, we chose a range of spectra of samples up to 1 μm for NH_3 deposited at 30 K and up to 2 μm of pure NH_3 and NH_3:N_2 ices at 15 K, for work in the MIR spectral region. The NIR region required a specific approach to treat the scattering effects (see next section), which allowed us to use larger thicknesses. We grew ice samples with thicknesses up to 3.5 μm for pure NH_3 at 15 K and 30 K and up to 8 μm for the mixture, because the absorption bands are very weak in this region. However, the temperature increased up to 25 K for the thicker films.

2.1. Optical Constants Calculation

In order to determine the complex refractive index $N_f = n - ik$ of thin solid films from normal incidence IR transmittance measurements, we used an analytical model of a three layer film-window-film transmission, based on the Fresnel equations, similar to that employed by Wood & Roux (1982), Toon et al. (1994), and Fernández-Torre et al. (2005). This model is presented in Appendix A. The procedure that we employed aims to iteratively minimize the difference between the experimental and calculated absorbance spectra of several thicknesses, using two merit functions, also defined in Appendix A. Only the main details are summarized here.

The need for oblique incidence spectra to evaluate optical constants from transmission data can be lifted if we assume that the ice material is isotropic (Baratta & Palumbo 1998), thus enabling the use of normal incidence spectra alone. We

have tested the validity of this approximation by recording IR spectra of our samples at oblique (30°) and normal incidence and detected no appreciable changes. The window layer is made of IR transparent silicon. The real component of its refractive index, $N_S(\nu)$, is taken from Frey et al. (2006) (note that the imaginary component, $k_S(\nu)$ vanishes for an IR transparent window). Since the thickness of the window (2 mm) is larger than the coherence length of the radiation, waves reflected in its front and back surfaces add incoherently. On the other hand, the ice layer cannot be described as too thin or too thick to allow for any approximations and a coherence parameter needs to be fit in the model for each film thickness.

The transmittance of thin films deposited on both sides of a substrate depends on several parameters, as indicated schematically in Equation (2):

$$T = f(N_f, N_S, d, c, \theta, \nu), \tag{2}$$

where N_f and N_S are the complex refractive indices of the film and the substrate, respectively, d is the film thickness, c is the degree of coherence of the film ($0 \leqslant c \leqslant 1$), θ is the angle of incidence (0° for normal incidence in our experiments), and ν is the wavelength of the radiation. The transmission of a three-layered system contains contributions of coherent and non-coherent interference. Whereas the substrate gives rise to non-coherent interference, the transmitted light through the two thin films is partly coherent and partly non-coherent. This system can be expressed by means of two transmission terms:

$$T = cT^{\mathrm{c}} + (1 - c)T^{\mathrm{nc}}, \tag{3}$$

where c is the degree of coherence of the ice film and T^{c} and T^{nc} are the coherent and non-coherent transmittance components, respectively. The expressions to calculate all these terms, based on Fresnel coefficients, are given in Appendix A.

The choice of a good initial guess for the iterative procedure is critical to ensure success. In particular, good estimates of the thickness of each sample and n_0 are needed. We derived the ice thicknesses and the n_0 values (1.36, 1.38, and 1.26) from our He–Ne laser interference fringe measurements, as described by Goodman (1978), and used them as a starting point to begin the numerical procedure. An initial value of the imaginary part of the refractive index $k(\nu)$ is calculated at each wavenumber using Lambert's law for the thickest film:

$$k(\nu) = \frac{1}{4\pi\nu d} A(\nu), \tag{4}$$

where $A(\nu)$ represents the absorbance at a given wavenumber, as defined in Appendix A. The corresponding $n(\nu)$ is then derived from the Kramers–Kronig equation:

$$n(\nu) = n_0 + \frac{2}{\pi} P \int_{\nu_1}^{\nu_2} \frac{\nu' k(\nu')}{\nu'^2 - \nu^2} d\nu', \tag{5}$$

where ν_1 and ν_2 define the range of frequency under consideration, 700 cm^{-1} and 4000 cm^{-1}, respectively, and P indicates the Cauchy principal value of the integral.

Using these initial values, the optimization procedure is set to refine $k(\nu)$ using the complete set of absorbance spectra as input data. From the improved values of $k(\nu)$, the real part of the complex index, $n(\nu)$, is estimated and the procedure is repeated until convergence is achieved. The second step includes an adjustable baseline subtraction from each spectrum to correct for spectral deformations due to scattering effects and a refinement of the corresponding coherence parameter. Next, n_0 and the sample thicknesses are adjusted to their final values. Finally, the final refined set of $n(\nu)$ and $k(\nu)$ values is obtained.

The n_0 values obtained at the end of the iteration procedure were 1.368 and 1.389 for pure NH_3 at 15 K and 30 K, respectively, and 1.261 for the NH_3:N_2 mixture. All refined values for the thickness and n_0 values agree with their experimental determinations within their estimated uncertainties.

We tried unsuccessfully to apply this same procedure to the NIR region. IR interference fringes dominate over NH_3 absorptions in this spectral zone and are affected by scattering, incoherence, and double reflections, which prevents us from using them for spectral reproduction. We took a different approach, inspired by Mastrapa et al. (2008), to determine the NIR optical constants of H_2O. We focused on the two spectral regions where NH_3 has absorption, i.e., the 6800–5900 cm^{-1} and 5200–4100 cm^{-1} intervals. In these regions, we subtracted an adequate baseline to remove IR interference. After this baseline subtraction, we calculated $k(\nu)$ using Equation (4) and averaged over the spectra of samples of the same phase and the same temperature, but different thicknesses. The averaged $k(\nu)$ values, together with previously determined values for the MIR range, were then used to derive $n(\nu)$ via the Kramers–Kronig relationship given in Equation (5).

Optical constants of these samples are very much in demand, but the band integrated absorbance values, A, are even more critically required. We calculated these band strengths for the MIR and NIR bands of NH_3 of the ices studied in this work using the imaginary part of the refraction index by means of the expression

$$A = \frac{4\pi}{\rho} \int k(\nu) \nu d\nu, \tag{6}$$

where ρ is the ice density. We have adopted a value of 0.76 g cm^{-3} determined by Wood & Roux (1982) for a temperature of 20 K for our samples of pure NH_3 ice at 15 K and 30 K. Recent measurements by Satorre et al. (2013) support this value. For the (NH_3:N_2) (1:1.7) ice mixture, based on a lack of better information, we assumed a density of 0.87 g cm^{-3}, which corresponds to the weighted average between the NH_3 density (0.76 g cm^{-3}) and that of N_2 (0.94 g cm^{-3}; Luna et al. 2012). The A value obtained for the mixture must be increased to take into account the fraction of NH_3 molecules in the sample in order to use this value as a reference for ammonia.

2.2. IR Spectra Calculations

Amorphous solids can be modeled using high quality computational methods. The validity of the models can be tested by comparing the predicted spectra with the corresponding experimental spectra. All calculations presented in this work were carried out using CASTEP, a module within the Materials Studio package (Segall et al. 2002), which is especially suitable for the treatment of solids, and allows the management of amorphous systems. Specific details of the theory and parameters used are given in Appendix B.

We studied pure amorphous ammonia ice and a mixture with nitrogen, in a 1:2 NH_3 to N_2 ratio, close to that used for our experiments. Our samples contain 32 NH_3 molecules inside a cubic cell for the former case and 8 NH_3 molecules with 16 N_2 molecules for the latter. Figure 8 in Appendix B shows a representation of the corresponding samples. After relaxation of the structure inside the cell, the vibrational spectrum can be predicted, within the usual restrictions, i.e., only the wavenumber

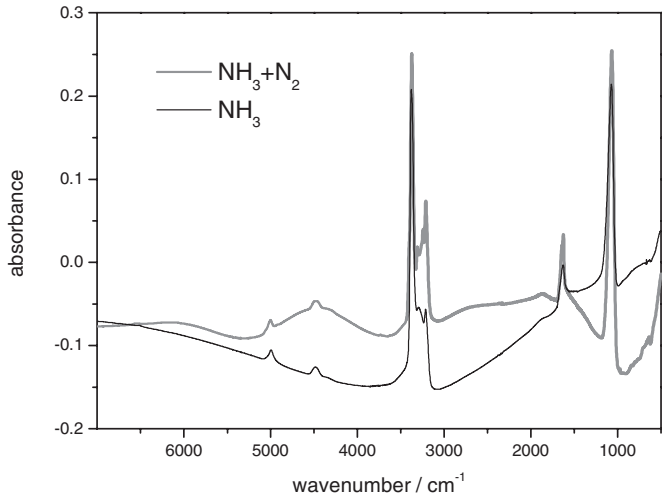

Figure 1. Composite of NIR and MIR spectra of a pure ammonia ice (black) and a 1:1.7 NH_3:N_2 ice mixture (gray) at 15 K. The thicknesses of the two ice samples are 700 nm and 2520 nm, respectively, but they contain the same number of NH_3 molecules.

and intensity of the fundamental modes are calculated, which leaves out some important spectroscopic information, such as anharmonic effects, band widths of the IR bands, and the NIR region where overtones and combination bands appear. This is unfortunate but the present state of the art does not allow these spectroscopic properties to be evaluated for solids, within our capabilities.

3. RESULTS

3.1. IR Spectra

Figure 1 shows the NIR and MIR spectra of pure ammonia ice and a NH_3:N_2 ice mixture (1:1.7) grown at 15 K. For each sample, the spectrum was recorded in two steps to cover the NIR and MIR spectral regions, which are represented together in the figure. The film thicknesses are ∼700 nm and ∼2520 nm for pure and mixed ice, respectively, as estimated from the measurements of the interference fringes of the He–Ne laser. Both samples contain the same number of ammonia molecules and the differences in the spectra are caused by the presence of nitrogen. The nitrogen molecule is IR inactive in the gas phase and the absorptions from pure N_2 ice is too weak to be seen for the thin film presented in Figure 1. The undulations visible in the baseline of the spectra are due to constructive and destructive interference of the IR radiation reflected in the ice layer and depend on the ice composition via the real part of the optical constant and the ice thickness. To facilitate the comparison of the different molecular absorptions in both spectra in Figure 2, we have subtracted adequate baselines drawn by eye to get rid of the IR interference.

The results are shown in Figures 2(a) and (b) where the assignment of the fundamental vibrations, in the MIR, and the combination modes, in the NIR, are also presented. These assignments are based on our calculations (see below) and confirm previous literature values (Reding & Hornig 1951).

Changes due to the presence of N_2 are appreciated in the band profile of some NH_3 absorptions, mainly in the ν_3, ν_4, and $\nu_3 + \nu_4$ modes that appear more structured and suffer small shifts (see Table 1 for frequency positions of the main peaks). We have also deposited amorphous ammonia ice at 30 K, but the corresponding spectrum exhibits very similar features as that of

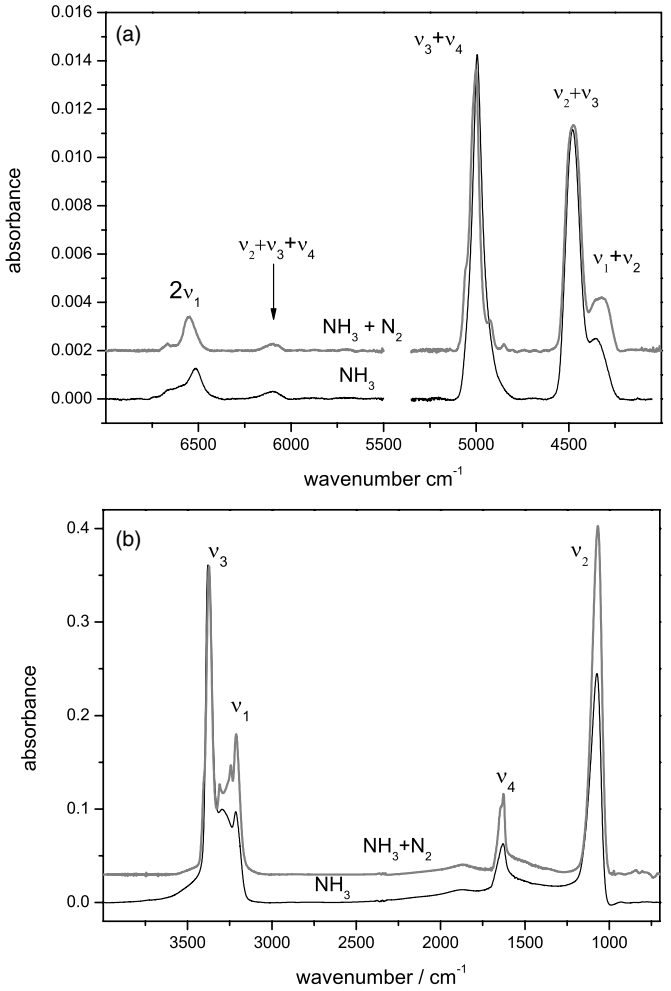

Figure 2. (a) NIR and (b) MIR spectra of the NH_3 (black) and the NH_3:N_2 1:1.7 ice mixture (gray) at 15 K presented in Figure 1, after subtraction of a baseline (see the text). The spectra of the mixture have been displaced vertically for clarity.

the 15 K NH_3 sample and is not shown in Figure 2. Simultaneous deposition of NH_3 and N_2 vapors at 30 K, with a pressure ratio $(P_{NH_3}/P_{N_2}) = (2.1 \times 10^{-5}$ mbar$/3.5 \times 10^{-5}$ mbar) were also performed. At this temperature, the sticking coefficient of N_2 is very low (Bisschop et al. 2006) and our observations show that the amount of N_2 condensed is not large enough to cause appreciable modifications in the spectrum of the pure ice, so it is not reproduced here either.

We carried out theoretical calculations to aid in the interpretation of the spectra presented in Figure 2. In the NIR spectral region, the bands correspond to combination modes that cannot be estimated with our calculation method. However, the MIR region can be compared in detail.

Figure 3 shows observed (panels a and c) and predicted (panels b and d) spectra for the systems mentioned above. Based on a lack of information on bandwidths, we have chosen to present the calculated spectra by means of Lorentzian lines with bandwidth values taken from the corresponding vibrations in the experimental spectra. Actual values are indicated in the figure caption. Several points are worth highlighting when comparing with observations. First, there is good agreement in frequency and intensity (except ν_1; see below) between experiments and theoretical simulations. Second, the frequency range (defined as the wavenumber interval in which similar

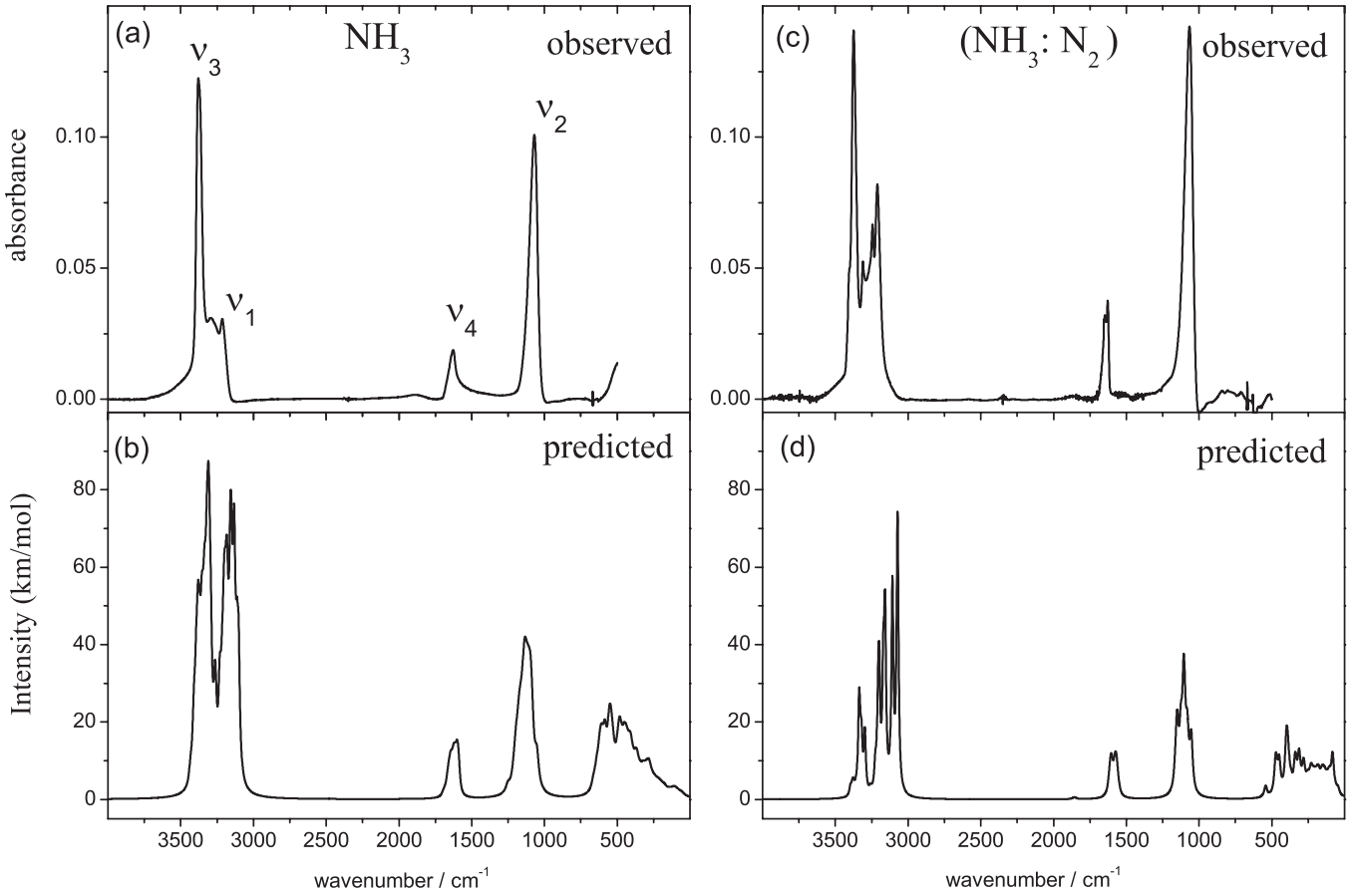

Figure 3. Comparison between observed spectra of (a) pure NH_3 and (c) a 1:1.7 NH_3:N_2 mixture at 15 K and the predicted spectra of (b) pure NH_3 and (d) a 1:2 NH_3:N_2 mixture. The calculated spectra were broadened with the following bandwidths: (b) 10 cm^{-1} for ν_3 and ν_1 and 16 cm^{-1} for ν_4 and ν_2; (d) 8 cm^{-1} for ν_3 and ν_1 and 12 cm^{-1} for ν_4 and ν_2.

Table 1
Observed Band Origins, ν_0 (in cm^{-1}), and Calculated Band Strengths, A (in cm $molecule^{-1}$), for Pure NH_3 at 30 K and 15 K and for a 15 K 1:1.7 Mixture of NH_3:N_2 (1:1.7)

Mode	NH_3				NH_3:N_2, 1:1.7		
	ν_0	This Work		Previous[a,b]	ν_0	This Work	Previous[c], 1:5
		A, 30K	A, 15K	A, 10 K		A, 15 K	A, 10 K
$2\,\nu_1$	6515	7.9×10^{-20}	6.3×10^{-20}	3.9×10^{-20} (4.2×10^{-20})[a]	6559	3.4×10^{-20}	9.5×10^{-20}
$\nu_2 + \nu_3 + \nu_4$	6094	1.3×10^{-20}	$\times 10^{-20}$	2.8×10^{-20} (3.0×10^{-20})[a]	6085	0.7×10^{-20}	
$\nu_3 + \nu_4$	4995	7.5×10^{-19}	7.3×10^{-19}	8.1×10^{-19} (8.8×10^{-19})[a]	5055, 5015, 5004, 4924, 4850	3.2×10^{-19}	4.4×10^{-19}
$\nu_2 + \nu_3$	4479	8.0×10^{-19}	7.1×10^{-19}	8.7×10^{-19} (9.4×10^{-19})[a]	4492, 4467	4.5×10^{-19}	2.4×10^{-19}
$\nu_1 + \nu_2$	4350				4352, 4298		
ν_3	3378	1.8×10^{-17}	1.5×10^{-17}	2.2×10^{-17} (2.9×10^{-17})[b]	3403, 3374, 3310, 3243	1.3×10^{-17}	
ν_1	3214				3210		
ν_4	1628				1646, 1628		
ν_2	1070	1.4×10^{-17}	1.3×10^{-17}	1.7×10^{-17} (2.2×10^{-17})[b]	1066	1.1×10^{-17}	

Notes. Where appropriate, the wavenumbers of split components are listed for the mixture.
[a] Gerakines et al. (2005); values in parentheses are re-scaled with the ν_2 band strength calculated in this work, $A_{1070} = 1.3 \times 10^{-7}$ cm $molecule^{-1}$.
[b] D'Hendecourt & Allamandola (1986); values in parentheses are corrected with the measured NH_3 ice density, $\rho = 0.76$ g cm^{-3} (Wood & Roux 1982).
[c] Richey & Gerakines (2012).

vibrational modes are calculated) spanned by each vibrational mode in the predicted spectrum of the mixture, is smaller than that of the corresponding mode in the pure amorphous case (range values are listed in Table 2), again with the exception of ν_1. This is again in accordance with the observed spectra. Third, ν_1 and ν_4 are split in several components in the observed spectrum of the nitrogen mixture, whereas they appear as broad features for pure ammonia, a characteristic reproduced also in the prediction. The last point can be interpreted if the presence of N_2 originated from more homogeneous or restricted environments for the NH_3 molecule, which gave rise to the observed narrower NH_3 absorption. Finally, in the predicted spectra, ν_1 appears stronger than ν_3, in contrast with the experiments, the gas phase spectrum of ammonia,

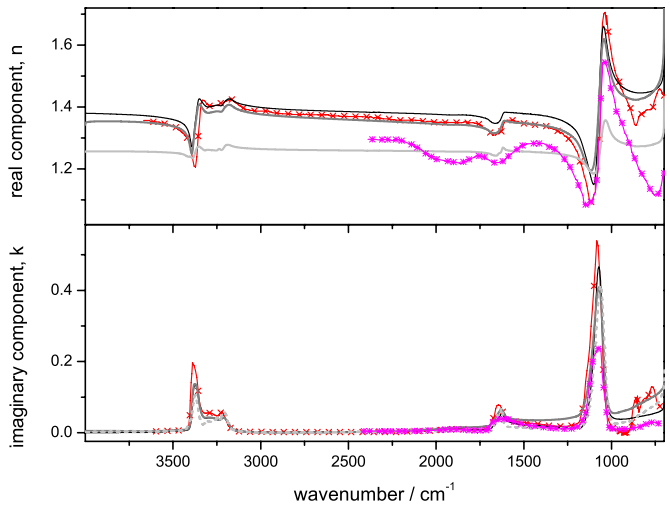

Figure 4. MIR optical constants of amorphous NH_3 at 30 K (black) and 15 K (dark gray), and a 1:1.7 NH_3:N_2 mixture at 15 K (light gray). The k values obtained for the mixture have been scaled to refer only to the NH_3 molecules (see the text). The optical constants given by Wood & Roux (1982; crosses, red) and Thompson et al. (1974; stars, magenta) for amorphous ammonia at 20 K and 30 K are also shown for comparison.

(A color version and supplemental data for this figure are available in the online journal.)

Table 2
Wavenumber Range, in cm^{-1}, of Calculated Vibrational Modes of Pure Amorphous Ammonia and Ammonia/Nitrogen Mixtures

Mode	NH_3	Range	NH_3/N_2	Range
ν_3	3435–3262	173	3397–3297	100
ν_1	3253–3102	151	3258–3072	186
ν_4	1698–1586	112	1620–1558	62
ν_2	1252–1052	200	1163–1054	109

and the calculations of pure ammonia crystals (research in progress). The Materials Studio software employed allows us to visualize atomic motions for each calculated vibrational mode. Examination of these motions reveals that several molecules vibrate in and out of phase in the ν_1 mode, regardless of their position in the amorphous structure. The corresponding local dipoles can be expected to be coupled and thus induce shifts in the corresponding wavenumbers and intensities. On the other hand, the most intense ν_3 modes correspond to individual molecules with negligible intermolecular couplings. The fact that this effect is not observed in the experimental spectra hints at some kind of molecular arrangement even at the low deposition temperature of our samples, which tends to cancel out ν_1 as a long-range outcome.

3.2. Optical Constants and Band Strengths

Figure 4 shows the real and imaginary components of the refractive index of amorphous ammonia ice at 15 K and 30 K in the MIR spectral region. The simulated spectra reproduce the experimental observations with a root mean square deviation of 0.001 in absorbance units. Figure 5 shows an example of this very good reproducibility. We estimate overall uncertainties of ∼1% for the real component of the refractive index n. The uncertainty is also ∼1% for the imaginary component, k, except when $k < 0.01$, which induces larger errors due to the larger signal-to-noise ratio in the film-substrate transmittance. Our results are compared in Figure 4 with previous literature data from Wood & Roux (1982), which correspond to NH_3 ice

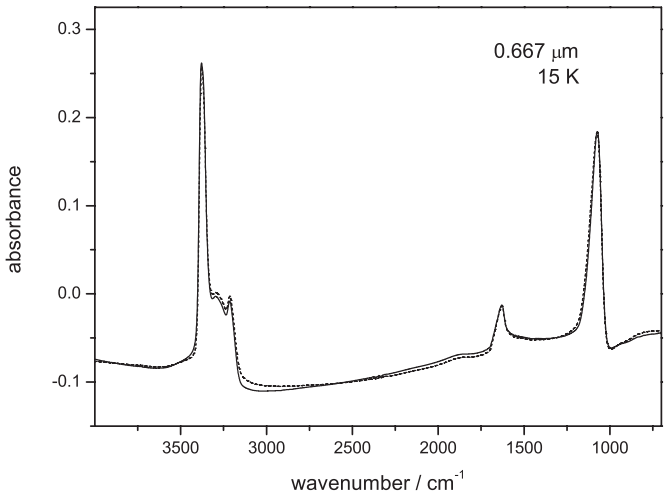

Figure 5. Comparison between experimental spectra (black line) of a 15 K NH_3 ice film 0.667 μm thick and that simulated with our optical constants (dashed line) given in Figure 4.

at 20 K. We also compare with data from Thompson et al. (1974) for NH_3 at 30 K. In both cases, the authors employed basically the same approach as used in this work to obtain the optical constants, although their spectra have a lower resolution (4 cm^{-1}). It can be seen that the global agreement between our constants and those of Wood & Roux is good, although the k maxima are a little lower in our estimations. The agreement with the results of Thompson et al. (1974) is not so good; their n and k values are below our estimations over the entire spectral range. At the absorption maximum at 1070 cm^{-1}, k is predicted to be around ∼14% higher for the 30 K sample than for the 15 K samples. This effect, although much amplified, was also observed for NH_3 ices grown at 20 K and 80 K by Roux et al. (1979), where k changed from 0.55 to 2.74.

Using the calculated indices n and k, we have determined the band strengths at 15 K of the two main absorptions, the "umbrella" ν_2 at 1070 cm^{-1} and the N–H stretchings ν_3 and ν_1 around 3300 cm^{-1}, $A_{1070} = 1.3 \times 10^{-17}$ cm molecule^{-1} and $A_{3375} = 1.5 \times 10^{-17}$ cm molecule^{-1}, respectively (see Table 1). Estimates for these band strengths were also reported by D'Hendecourt & Allamandola (1986) from measurements of a single spectrum of a 0.74 μm thick sample. As far as we know, no other estimates of the absolute band strengths of pure amorphous NH_3 ice are available. The values published by these authors were 1.7×10^{-17} cm molecule^{-1} and 2.2×10^{-17} cm molecule^{-1} for A_{1070} and A_{3375}, respectively, but these values were obtained under the assumption of a 1 g cm^{-3} density for the amorphous ammonia ice. If we correct the density to the measured value of 0.76 g cm^{-3} (Wood & Roux 1982), the band strengths of D'Hendecourt & Allamandola transform into 2.2×10^{-17} cm molecule^{-1} and 2.9×10^{-17} cm molecule^{-1}, respectively, which are appreciably larger than the values determined in this work. The present results, based on a detailed analysis of multiple samples and using the experimental density for NH_3 ice, are deemed to be more accurate.

As discussed above, the 1070 cm^{-1} (9.34 μm) umbrella band of ammonia, which does not overlap with any H_2O absorption, is the most suitable feature for astronomical observations of ammonia-containing ices. Kerkhof et al. (1999) have shown that the intensity of this band decreases in mixtures of NH_3 with water ice, up to values as much as 30% for high ammonia dilutions. Kerkhof et al. (1999) did not measure absolute band

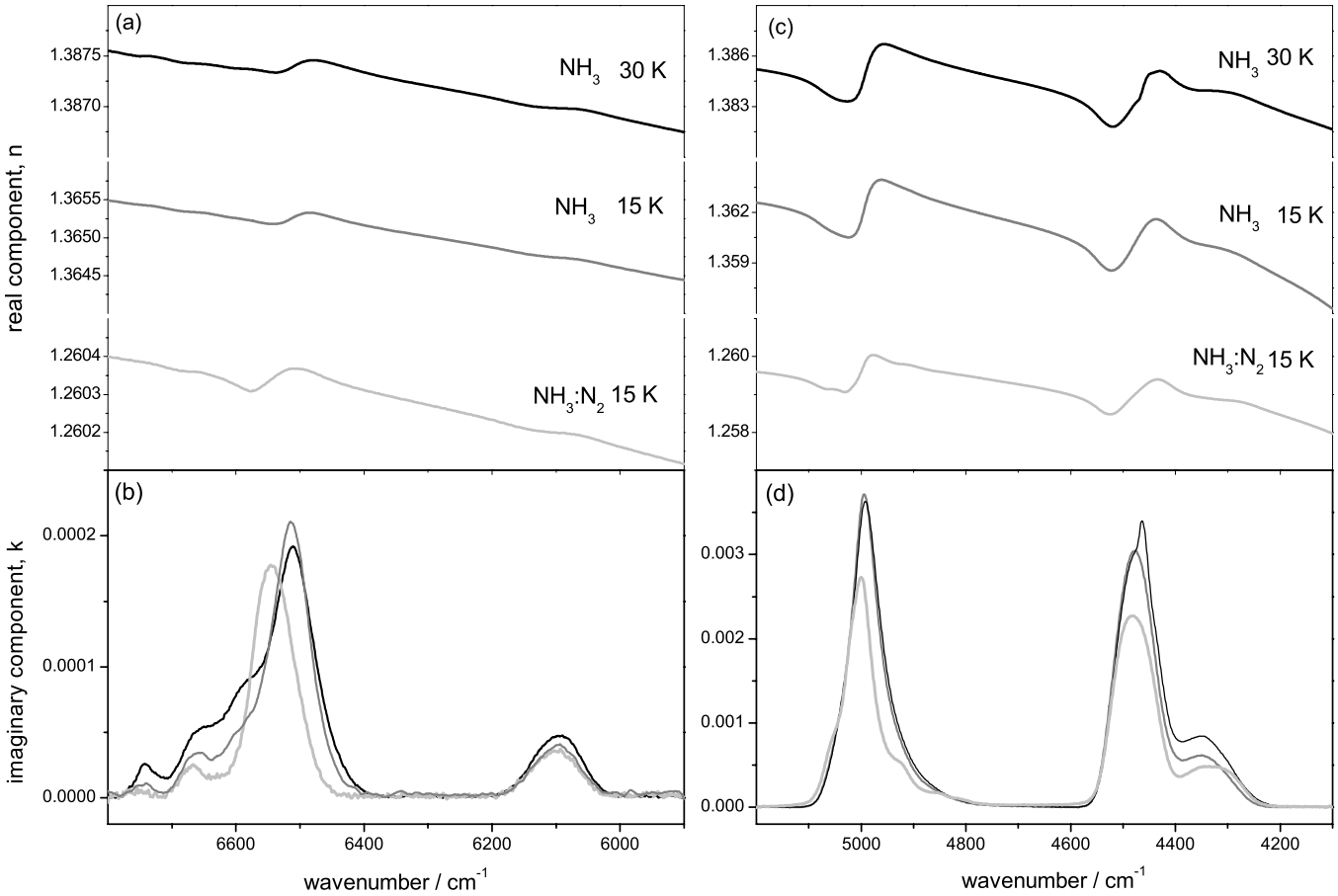

Figure 6. NIR optical constants for pure NH_3 at 30 K (black) and 15 K (dark grey) and a 1:1.7 NH_3:N_2 mixture at 15 K (light grey; the k values obtained for the mixture have been scaled to refer only to the NH_3 molecules; see the text). Real component: panels a and c: NH_3 30 K, NH_3 15 K, and NH_3:N_2 15 K. Imaginary components: panel b and d.

(Supplemental data for this figure are available in the online journal.)

strengths but provided A_{1070} estimates for various NH_3/H_2O proportions using the value of D'Hendecourt & Allamandola (1.7×10^{-17} cm molecule^{-1}) as a reference.

Figure 6 shows the optical constants in the NIR spectral region for the ammonia ices studied in this work. Notice that the k values are below 0.004 (0.0003) for the 4500 cm^{-1} (6500 cm^{-1}) region. The estimated absolute uncertainties for these magnitudes are ∼30% and ∼60%, respectively, mainly due to errors in the subtraction of the appropriate baseline. Nevertheless, the relative uncertainty between measurements is well below these values, which allows information on peak positions and band shapes to be extracted. It is interesting to appreciate the particular behavior of the band at ∼ 4479 cm^{-1} ($\nu_2 + \nu_3$) that develops a narrow peak in the NH_3 ice at 30 K, a feature that is not present in any other ices grown at 15 K. This narrow peak starts to appear for ice thicknesses above 1 μm and is believed to be related to morphology effects, as pointed out by other authors (Dawes et al. 2007; see below). For the ice mixture, the main difference compared with pure ice is the appearance of some structure in the ∼ 5000 cm^{-1} band and a shift of the main peak of the ∼ 6515 cm^{-1} absorption. The IR optical constants presented here are a useful tool for interpreting different kinds of spectroscopic observations in various astronomical environments, ranging from the ISM to the outer solar system. In particular, they might contribute to the detection of ammonia in cold trans-Neptunian objects or even in the ices of Saturnian moons like Ione, Iapetus, or Titan, where the presence of ammonia is expected but has not yet been confirmed (Dalton 2010).

From these optical constants, we have extracted the absolute band strengths by applying Equation (6), with the results listed in Table 1. The present band strengths can be compared with those of Gerakines et al. (2005) and Richey & Gerakines (2012) for pure NH_3 ice and a 1:5 NH_3:N_2 mixture. Band strengths in the NIR are usually estimated by referencing measured values in the MIR; the choice of the reference can lead to controversial results. The values given in Gerakines et al. (2005) and Richey & Gerakines (2012) were scaled to an estimation by Kerkhof et al. (1999) of $A_{1070} = 1.2 \times 10^{-17}$ cm molecule^{-1}, which nearly agrees with the $A_{1070} = 1.3 \times 10^{-17}$ cm molecule^{-1} value derived in the present work. This agreement is in fact fortuitous since the A_{1070} value of Kerkhof et al. (1999) corresponds to highly diluted (1/44) NH_3 in water ice. We re-scaled the values of Gerakines et al. (2005) with our A_{1070} estimation for consistency in the comparison. The re-scaled values are quoted in parentheses in Table 1. The agreement between the present results and those of Gerakines et al. (2005) is good (within 25%) for the two absorption features below 5000 cm^{-1}. Larger differences are observed for the much smaller A values of the two features beyond 6000 cm^{-1}. Taban et al. (2003), on the other hand, reported a band strength of 9.7×10^{-19} cm molecule^{-1} for the 4471 cm^{-1} absorption of pure NH_3 ice at 12 K, using as a reference the MIR

$A_{1070} = 1.7 \times 10^{-17}$ cm molecule^{-1} value of D'Hendecourt & Allamandola (1986). If we use the present band strength $A_{1070} = 1.3 \times 10^{-17}$ cm molecule^{-1} for the scaling, the result of Taban et al. (2003) transforms into 7.4×10^{-19} cm molecule^{-1}, in very good agreement with our data.

An overall intensity decrease of the IR absorption of NH_3 in the mixtures is observed compared with the pure samples (see Table 1). This attenuation is larger for the combination bands in the NIR spectral region. Our results confirm this behavior that was already observed by Richey & Gerakines (2012), for a more diluted (1:5) NH_3:N_2 mixture (see Table 1).

Absolute band strength values derived from laboratory experiments have been used for the determination of NH_3 relative abundances in interstellar ices (see Bottinelli et al. 2010 and references therein). As indicated above, the 1070 cm^{-1} MIR absorption has been the usual choice for these estimations, but NIR features have also been occasionally used to set upper limits on the NH_3 concentration (Taban et al. 2003). In the recent and very thorough c2d *Spitzer* spectroscopic survey (Bottinelli et al. 2010; Öberg et al. 2011), an average NH_3 relative abundance of $\sim 5\%$ with respect to H_2O was obtained from observations toward both high-mass and low-mass protostars. For this estimate, a band strength $A_{1070,\mathrm{diluted}} = 1.3 \times 10^{-17}$ cm molecule^{-1} was used. This corresponds to the value of Kerkhof et al. (1999) for NH_3 highly diluted in H_2O ice. As commented on previously, no absolute band strengths were measured by Kerkhof and coworkers and the relative values for the various NH_3:H_2O mixtures studied were scaled to the $A_{1070,\mathrm{pure}} = 1.7 \times 10^{-17}$ cm molecule^{-1} value reported by D'Hendecourt & Allamandola (1986) for pure NH_3 ice. The results of the present work indicate that a more accurate value for the pure NH_3 ice band strength is $A_{1070,\mathrm{pure}} = 1.3 \times 10^{-17}$ cm molecule^{-1}. Rescaling the data of Kerkhof et al. (1999) with this new value would lead to smaller $A_{1070,\mathrm{diluted}}$ values for NH_3 in water ice and thus to higher concentrations of ammonia. In particular, the estimates from the c2d survey of ammonia in ice should be scaled upward by $\sim$30%. It should be borne in mind that NH_3 is one of the main nitrogen carriers in interstellar space and, as such, one of the key molecules in astrochemical networks leading to more complex N-bearing species and ultimately to prebiotic molecules. The appreciable increase in the estimated NH_3 ice reservoir deduced from our measurements should thus be relevant for astrochemical models of protostellar objects from the cold initial steps, where NH_3 is mainly involved in ice chemistry, to the hotter stages where ammonia and its derivatives desorb from the grains and react further in the gas phase.

3.3. Thermal Processing: N_2 Effect

Thermal processing of the pure NH_3 ices and NH_3:N_2 mixtures was carried out by heating the ices at a controlled rate of 5 K minute^{-1}. It is well established that an amorphous phase of ammonia is obtained when samples are prepared below 50 K and that a crystalline phase (polycrystalline) is obtained when heating above 80 K. Dawes et al. (2007) conducted a detailed study on the morphology and phases of solid ammonia films based on vacuum ultraviolet and IR spectroscopy and concluded that the IR spectrum of a polycrystalline ice film is largely influenced by the size and shape of the crystalline domains obtained, which in turn depend strongly on the generation conditions. Ices grown at $T < 50$ K, like in our experiments, are amorphous. When these ice samples are heated above the crystallization temperature (80 K), the ν_2 and ν_3 bands of NH_3 split into several peaks, which were associated with a polycrystalline sample with crystallites of random sizes and shapes by Dawes et al. (2007). This effect is reproduced for our pure NH_3 ice samples when warmed to 85 K (see Figure 7, bottom panels, black line). However, the spectra of ice mixtures containing N_2 undergo different changes after being heated to 85 K, induced by the release of volatile N_2 during this process (Figure 7, bottom panels, grey line). In particular, ν_2 presents a narrow peak and a shoulder, resembling the spectrum attributed by Dawes et al. (2007) to a sample consisting of large crystallites, formed by direct deposition of NH_3 vapor at temperatures above 85 K. Making use of their interpretation of the spectra, our results lead us to conclude that the formation of large crystallite domains in the ice film is favored by the presence of N_2, either by facilitating the mobility of the NH_3 molecules or by providing some energy from the release associated with the sublimation of N_2.

Ammonia has been detected on the surface of some icy objects of our solar system, that may also contain N_2 and other volatiles buried underneath. The spectra presented here could help in the interpretation of the history of the surface of these objects, since, as we show, the phase of NH_3 is affected not only by the temperature reached by the ice but also by eruptions of trapped volatiles coming from lower layers.

4. SUMMARY AND CONCLUSIONS

This work presents a detailed study of amorphous NH_3 ice and NH_3:N_2 ice mixtures based on IR spectra in the MIR and NIR regions, supported by theoretical quantum chemical calculations. By recording spectra of samples of varying thickness, we have been able to derive the optical constants of amorphous ammonia at 15 K and 30 K and the mixtures at 15 K in both spectral regions, with improved accuracy over previous data, where available. Using the imaginary part of the refractive index and a good estimation of the density of our samples, we have also obtained absolute values of the band strengths of the more important IR features in both spectral regions.

The main conclusions and astrophysical implications of this work are therefore the following.

1. The optical indices of ammonia ice and mixtures with N_2 that we provide in this paper revise and complement previous results. In the astrophysical community, these data are of crucial relevance, especially for the simulation of IR diffuse reflection spectra obtained in observations of solar system external bodies.
2. The concentration of NH_3 ice in the ISM has been evaluated from observations of the 1070 cm^{-1} band (Bottinelli et al. 2010; Öberg et al. 2011). These authors estimate roughly 5% NH_3 with respect to water in the ices of high- and low-mass protostars, based on the previously reported laboratory IR band strength for this absorption. We present an improved value for this band strength, $A_{1070} = 1.3 \times 10^{-17}$ cm molecule^{-1} (with about 10% estimated uncertainty), which is approximately 30% smaller than the previous result. Consequently, the revised NH_3 concentration for ISM ices should be 6.5% with respect to water. This estimated increase should be relevant in chemical networks involving N in protostellar objects.
3. Ammonia ice gives rise to a NIR feature at 4479 cm^{-1}, in a zone free of water absorption that can be used also for the estimation of the amount of ammonia in ISM ices (Taban et al. 2003). This band is more than two orders of magnitude

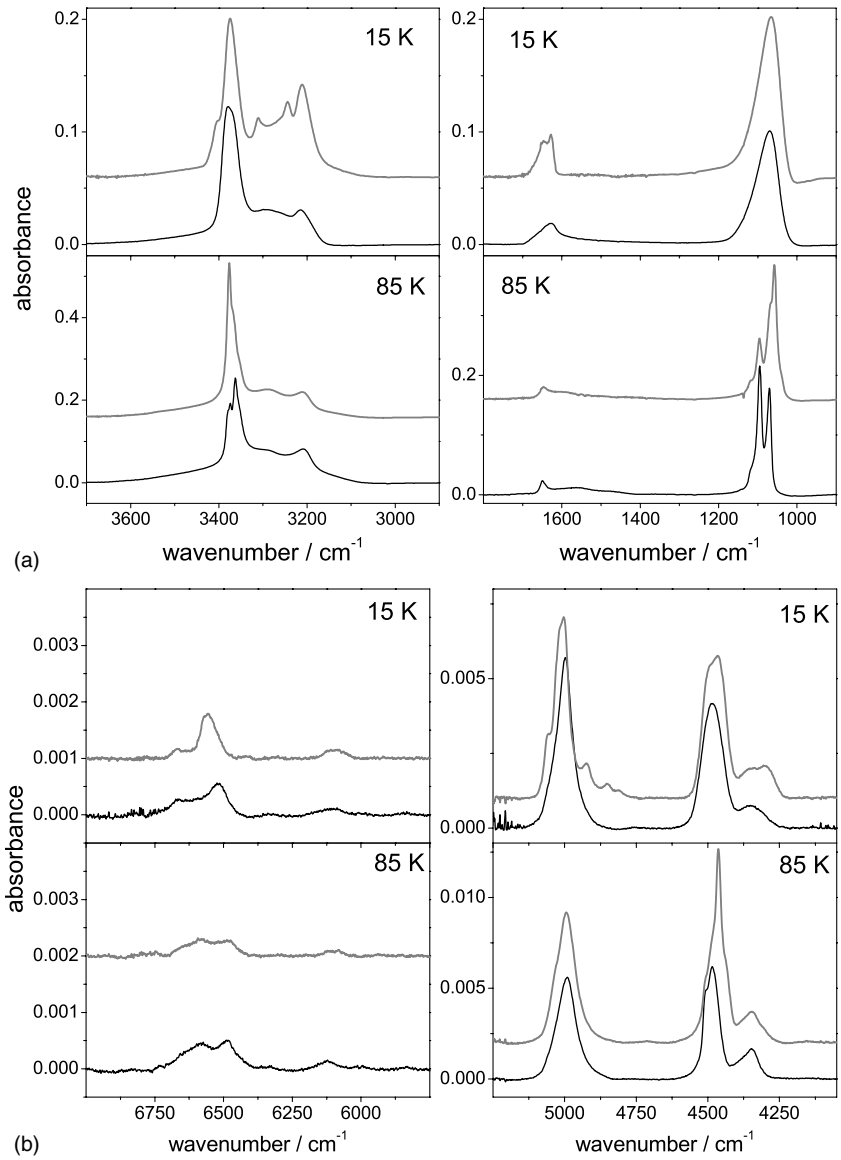

Figure 7. (a) MIR and (b) NIR bands of ammonia in a pure NH_3 (black) and NH_3:N_2 (gray) ice deposited at 15 K. Top panels: 15 K. Bottom panels: 85 K, after heating the ices at 5 K minute^{-1}.

weaker than other features in the MIR. Our assessment for the strength of this band, which is affected by a poorer estimated uncertainty, is in good agreement with that of Taban et al. (2003) and agrees with that of Gerakines et al. (2005) within our error limits, ∼30%.

4. We have investigated in detail the effect of the presence of N_2 in ammonia ices. The observed band contour changes and small frequency shifts can be used as indirect evidence for the existence of N_2 in astrophysical media. This technique has already been used for the detection of N_2 in methane matrices, as discussed in the Introduction.
5. The crystallization of amorphous ammonia ice is a complex process that is also affected by the presence of N_2 in the sample. The data presented here for the thermal evolution of our samples can be interesting for the interpretation of the history of icy bodies in the solar system.

This research has been carried out with funding from the Spanish Ministry of Education, Projects FIS2010–16455, and CTQ-2008–02578/BQU. O.G. and Y.R.-L. acknowledge financial support from Ramón y Cajal Program and CSIC, JAE-Doc Program, respectively. We thank Javier Fochesatto for a careful reading of the manuscript.

APPENDIX A

A.1. Fresnel Model for a Three Layer Film-substrate-film Set Up

Our system is composed of film 1, a thick substrate S, and film 2. In the following, 1 and 2 refer to the ice films (of equal thickness), 0 refers to air, and S refers to the substrate. N_f is a complex magnitude and N_S is real. The absorbance at a given wavelength is defined by the ratio of the transmittance T of the three layered system to that of the bare substrate, T_S:

$$A(\nu) = -\log\left(\frac{T(\nu)}{T_S(\nu)}\right). \quad \text{(A1)}$$

The bare substrate transmission is given by

$$T_S = \frac{T_{0S}T_{S0}}{1 - R_{S0}^2}, \tag{A2}$$

where $T_{ij} = 1 - R_{ij}$, $R_{ij} = |r_{ij}|^2$, and r_{ij} are the Fresnel coefficients for reflection in the interface between layers i and j (Heavens 1995).

The three layer coherent ($X = $ c) or non-coherent ($X = $ nc) normal incidence transmission is given by

$$T^X = \frac{T_{f1}^X T_{f2}^X}{1 - R_{f1}^X R_{f2}^X}, \tag{A3}$$

where the composite transmission and reflection factors can be written as (Fernández-Torre et al. 2005; Heavens 1995)

$$T_{f1}^{\rm c} T_{f2}^{\rm c} = \left| \frac{t_{01}t_{1S}e^{i\delta_1}}{1 + r_{01}r_{1S}e^{i(2\delta_1 - \varphi_1)}} \right|^2 \left| \frac{t_{S2}t_{20}e^{i\delta_2}}{1 + r_{S2}r_{20}e^{i(2\delta_2 - \varphi_2)}} \right|^2$$

$$R_{f1}^c = |\frac{r_{1s} + r_{01}e^{i(2\delta_1 - \varphi_1)}}{1 + r_{1s} + r_{01}e^{i(2\delta_1 - \varphi_1)}}|^2 \tag{A4}$$

$$R_{f2}^{\rm c} = \left| \frac{r_{S2} + r_{20}e^{i(2\delta_2 - \varphi_1)}}{1 + r_{S2}r_{20}e^{i(2\delta_2 - \varphi_1)}} \right|^2$$

and

$$T_{f1}^{\rm nc} T_{f2}^{\rm nc} = \frac{T_{01}T_{1S}e^{-2{\rm Im}(\delta_1)}}{1 - R_{01}R_{1S}e^{-2{\rm Im}(2\delta_1 - \varphi_1)}} \frac{T_{S2}T_{20}e^{-2{\rm Im}(\delta 2)}}{1 - R_{S2}R_{20}e^{-2{\rm Im}(2\delta_2 - \varphi_1)}}$$

$$R_{f1}^{\rm nc} = R_{1S} + \frac{T_{S1}T_{1S}R_{01}e^{-2{\rm Im}(2\delta_1 - \varphi_1)}}{1 - R_{1S}R_{01}e^{-2{\rm Im}(2\delta_1 - \varphi_1)}}, \tag{A5}$$

$$R_{f2}^{\rm nc} = R_{S2} + \frac{T_{S2}T_{2S}R_{20}e^{-2{\rm Im}(2\delta_2 - \varphi_1)}}{1 - R_{S2}R_{20}e^{-2{\rm Im}(2\delta_2 - \varphi_1)}},$$

with phases in normal incidence given by

$$2\delta_1 - \varphi_1 = 2\delta_{12} - \varphi_1 = \frac{4\pi}{l} dN_f;$$
$$\delta_1 = \delta_2 = \frac{2\pi}{l} dN_f. \tag{A6}$$

A.2. Refinement Procedure

The procedure to derive the optical constants of our systems minimizes iteratively the difference between the experimental and calculated absorbance spectra of samples of several thicknesses by employing two merit functions, which we have called M and W.

The function $M(\nu)$ gives, for a particular wavelength, the square of the difference between the experimental and the simulated absorbance, weighted by the sample thickness, and summed over all spectra:

$$M(\nu) = \sum_1^{n_d} \frac{(A_{\rm exp}(\nu) - A_{\rm theo}(\nu))^2}{d}, \tag{A7}$$

where n_d is the number of spectra used. Weighting by the respective thickness is included to take into account the different relative errors for each spectrum. The function W calculates the quadratic error summed over the frequency range of the experiments:

$$W(\nu) = \sum_{\nu_1}^{\nu_2} (A_{\rm exp}(\nu) - A_{\rm theo}(\nu))^2, \tag{A8}$$

where ν_1 and ν_2 define the frequency interval we want to consider. The minimization of these functions, for the different variables, is done using the steepest descent method, as described by Verleur (1968). As the number of variables is large, M and W define hypersurfaces that present several local minima. The iterative minimization procedure can converge to any local minima that do not necessarily correspond to the global minimum associated with the correct solution. To reach the absolute minimum, the steps described below have been followed. We should note here that this procedure is not unique and has to be adapted in cases of poor convergence.

Once the initial conditions are chosen, the so-called K–K iterative procedure is applied. It consists of the minimization of the merit function M by optimizing $k(\nu)$ at each wavenumber, using the complete set of spectra with different thicknesses. After an optimization, the improved set of $k(\nu)$ values is used to calculate the $n(\nu)$ values by means of the K–K procedure (Equation (5)). Then, the M function is minimized again and the procedure is repeated, usually converging in a few iterations.

In the second stage, the offset of each experimental spectrum is estimated and the coherence factor is optimized. The offset correction is applied by subtracting a linear background from each spectrum, evaluating the a and b coefficients that minimize the difference between the corrected experimental spectrum and the simulated one, i.e., searching for the minimum of the expression $[A_{\rm exp} - (a\nu + b) - A_{\rm theo}]$. Then, the merit function W is minimized by refining the coherence coefficient for each thickness. To do this, only the frequency intervals that are free of strong absorption are considered. With the new coherence parameter, a fresh estimation of the experimental offsets a and b of each spectrum is conducted. These two stages are repeated until convergence is achieved, normally after three iterations.

The third stage involves the refinement of n_0 and the thicknesses, applying usually a minor correction over the estimated values. The optimization of n_0 is performed by minimizing the product of the merit functions M and W. Then, the thicknesses are adjusted by minimizing the merit function W for each spectrum. Finally, the K–K iterative procedure is applied again to yield the refined set of $n(\nu)$ and $k(\nu)$ values adapted to the optimized n_0 and d values.

APPENDIX B

We have used density functional theory with the generalized gradient approximation and PBE functionals (Perdew et al. 1996). Convergence tolerance parameters were 1.0×10^{-5} eV atom^{-1}, 0.03 eV Å^{-1}, 0.05 GPa, and 0.001 Å for energy, force, stress, and atomic displacement, respectively, for amorphous NH_3. The corresponding values were 5.0×10^{-6} eV atom^{-1}, 0.01 eV Å^{-1}, 0.02 GPa, and 5×10^{-4} Å for the mixture.

Our samples contain 32 NH_3 molecules inside a cubic cell of 0.85 g cm^{-3} density for the former case and 8 NH_3 molecules with 16 N_2 molecules with a density of 1 g cm^{-3} for the latter case. Figure 8 shows a representation of the corresponding samples.

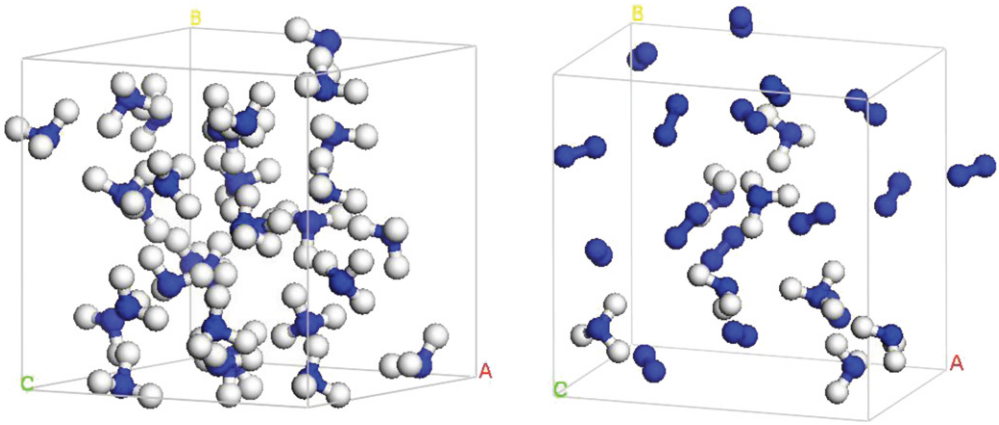

Figure 8. Amorphous ammonia cell (left) and 1:2 NH_3:N_2 mixture (right). H atoms are represented by white spheres and N atoms are shown as blue spheres.
(A color version of this figure is available in the online journal.)

REFERENCES

Baratta, G. A., & Palumbo, M. E. 1998, JOSAA, 15, 3076
Bauer, J. M., Roush, T. L., Geballe, T. R., et al. 2002, Icar, 158, 178
Bisschop, S. E., Fraser, H. J., Öberg, K. I., van Dishoeck, E. F., & Schlemmer, S. 2006, A&A, 449, 1297
Bottinelli, S., Boogert, A. C. A., Bouwman, J., et al. 2010, ApJ, 718, 1100
Brown, M. E., & Calvin, W. M. 2000, Sci, 287, 107
Cheung, A. C., Rank, D. M., Townes, C. H., Thornton, D. D., & Welch, W. J. 1968, PhRvL, 21, 1701
Cochran, A. L., & Cochran, W. D. 1981, Icar, 48, 488
Cruikshank, D. P., Roush, T. L., Owen, T. C., et al. 1993, Sci, 261, 742
Dalton, J. B. 2010, SSRv, 153, 219
Dalton, J. B., Cruikshank, D. P., Stephan, T. B., et al. 2010, SSRv, 153, 113
Dawes, A., Mukerji, R. J., Davis, M. P., et al. 2007, JChPh, 126, 244711
D'Hendecourt, L. B., & Allamandola, L. J. 1986, A&AS, 64, 453
Douté, S., Schmitt, B., Quirico, E., et al. 1999, Icar, 142, 421
Emery, J. P., Burr, D. M., Cruikshank, D. P., Brown, R. H., & Dalton, J. B. 2005, A&A, 435, 353
Fernández-Torre, D., Escribano, R., Herrero, V. J., et al. 2005, JPCB, 109, 18010
Frey, B. J., Leviton, D. B., & Madison, T. J. 2006, Proc. SPIE, 6273, 62732J
Gerakines, P. A., Bray, J. J., Davis, A., & Richey, C. R. 2005, ApJ, 620, 1140
Goodman, A. M. 1978, ApOpt, 17, 2779
Grundy, W. M., Schmitt, B, & Quirico, E. 1993, Icar, 105, 254
Heavens, O. S. 1995, Optical Properties of Thin Solid Films (London: Butterworth Scientific Publications)
Herrero, V. J., Gálvez, O, Maté, B., & Escribano, R. 2010, Phys. Chem. Chem. Phys., 12, 3164
Hofstadter, M. D, & Muhleman, D. O. 1989, Icar, 81, 396
Holt, J. S., Sadoskas, D., & Pursell, C. J. 2004, JChPh, 120, 7153
Howett, C. J. A., Carlson, R. W., Irwin, P. G. J., & Calcutt, S. B. 2007, JOSAB, 24, 126
Jewitt, D. C., & Luu, J. 2004, Natur, 432, 731
Kerkhof, O., Schutte, W. A., & Ehrenfreund, P. 1999, A&A, 346, 990
Licandro, J., Grundy, W. M., Pinilla-Alonso, N., & Leisy, P. 2006a, A&A, 458, L5
Licandro, J., Pinilla-Alonso, N., Pedani, M., et al. 2006b, A&A, 445, L35
Lindal, G. F. 1992, ApJ, 103, 967
Luna, R., Satorre, M. A., Domingo, M, Millán, C, & Santonja, C. 2012, Icar, 221, 186
Mastrapa, R. M., Bernstein, M. P., Sandford, S. A., et al. 2008, Icar, 197, 307
Maté, B., Medialdea, A., Moreno, M. A., Escribano, R., & Herrero, V. J. 2003, JPCB, 107, 11098
Moore, M. H., Ferrante, R. F., Hudson, R. L., & Stone, J. N. 2007, Icar, 190, 260
Öberg, K. I., Boogert, A. C. A., Pontoppidan, K. M., et al. 2011, ApJ, 740, 109
Perdew, J. P., Burke, K., & Ernzerhof, M. 1996, PhRvL, 77, 3865
Pipes, J. G., Roux, J. A., & Smith, A. M. 1978, AIAAJ, 16, 984
Quirico, E., Doute, S., Schmitt, B., et al. 1999, Icar, 139, 159
Quirico, E., & Schmitt, B. 1997, Icar, 127, 354
Reding, F. P., & Hornig, D. F. 1951, JChPh, 19, 594
Richey, C. R., & Gerakines, P. A. 2012, ApJ, 759, 74
Robertson, C. W., Dowing, H. D., Curnutte, B., & Williams, D. 1975, JOSA, 65, 432
Roux, J. A., Wood, B. E., & Smith, A. M. 1979, AEDC-TR-79–57 (AD-A074913)
Satorre, M. Á., Leliwa-Kopystynski, J., Santonja, C., & Luna, R. 2013, Icar, 225, 703
Segall, M. D., Lindan, P. J. D., Probert, M. J., et al. 2002, JPCM, 14, 2717
Snow, T. P., & Witt, A. N. 1996, ApJL, 468, L65
Taban, I. M., Schutte, W. A., Pontoppidan, K. M., & van Dishoeck, E. F. 2003, A&A, 399, 169
Thompson, S. B., Arnold, F., Sanderson, R. B., & Monty, A. W. 1974, in Thermophysics and Spacecraft Thermal Control, Optical Properties of Cryodeposits on Low Scatter Mirrors, ed. R. C. Hening (Progress in Aeronautics and Astronautics, Vol. 35; Cambridge, MA: MIT), 229
Toon, O. B., Tolbert, M. A., Koehler, B. G., Middlebrook, A. M., & Jordan, J. 1994, JGR, 99, 25631
Verleur, H. W. 1968, JOSA, 58, 1356
Wong, M. H., Bjoraker, G. L., Smith, M. D., Flasar, F. M., & Nixon, C. A. 2004, P&SS, 52, 385
Wood, B. E., & Roux, J. A. 1982, JOSA, 72, 720
Zheng, W., Jewitt, D., & Kaiser, R. I. 2009, ApJS, 181, 53
Zheng, W., & Kaiser, R. I. 2007, CPL, 440, 229